MOLECULAR AND CELLULAR BIOLOGY, Apr. 2009, p. 1869–1881 Vol. 29, No. 7
0270-7306/09/$08.00+0 doi:10.1128/MCB.01089-08

p31 Deficiency Influences Endoplasmic Reticulum Tubular Morphology and Cell Survival[▽]

Takefumi Uemura,[1,2]† Takashi Sato,[1]† Takehiro Aoki,[2] Akitsugu Yamamoto,[3] Tetsuya Okada,[4] Rika Hirai,[1] Reiko Harada,[1] Kazutoshi Mori,[4] Mitsuo Tagaya,[2]* and Akihiro Harada[1,5]*

Laboratory of Molecular Traffic, Department of Molecular and Cellular Biology, Institute for Molecular and Cellular Regulation, Gunma University, Maebashi, Gunma 371-8512, Japan[1]; School of Life Sciences, Tokyo University of Pharmacy and Life Sciences, Hachioji, Tokyo 192-0392, Japan[2]; Department of Cell Biology, Nagahama Institute of Bio-Science and Technology, Nagahama, Shiga 526-0829, Japan[3]; Department of Biophysics, Graduate School of Science, Kyoto University, Sakyou-ku, Kyoto 606-8502, Japan[4]; and Department of Cell Biology, Graduate School of Medicine, Osaka University, 2-2 Yamada-oka, Suita, Osaka 565-0871, Japan[5]

Received 10 July 2008/Returned for modification 4 September 2008/Accepted 10 January 2009

p31, the mammalian orthologue of yeast Use1p, is an endoplasmic reticulum (ER)-localized soluble *N*-ethylmaleimide-sensitive factor attachment protein (SNAP) receptor (SNARE) that forms a complex with other SNAREs, particularly syntaxin 18. However, the role of p31 in ER function remains unknown. To determine the role of p31 in vivo, we generated *p31* conditional knockout mice. We found that homozygous deletion of the *p31* gene led to early embryonic lethality before embryonic day 8.5. Conditional knockout of *p31* in brains and mouse embryonic fibroblasts (MEFs) caused massive apoptosis accompanied by upregulation of ER stress-associated genes. Microscopic analysis showed vesiculation and subsequent enlargement of the ER membrane in p31-deficient cells. This type of drastic disorganization in the ER tubules has not been demonstrated to date. This marked change in ER structure preceded nuclear translocation of the ER stress-related transcription factor C/EBP homologous protein (CHOP), suggesting that ER stress-induced apoptosis resulted from disruption of the ER membrane structure. Taken together, these results suggest that p31 is an essential molecule involved in the maintenance of ER morphology and that its deficiency leads to ER stress-induced apoptosis.

The endoplasmic reticulum (ER) consists of a network of tubules and sheets that extends from the cell center to the periphery in eukaryotic cells. It synthesizes secretory and membrane proteins as well as lipids. In addition, the ER has many diverse functions, including folding, posttranslational modification, export of secretory and membrane proteins, and calcium storage. Various intracellular and extracellular stimuli, including reduction of disulfide bonds, calcium depletion from the ER lumen, inhibition of glycosylation, and impairment of protein transport from the ER to the Golgi complex, affect functions of the ER, and disturbance in ER functions causes ER stress. In case of prolonged ER stress, cellular signaling leading to cell death are activated. ER stress has been suggested to be involved in various disorders (12, 19, 36).

The ER maintains several functionally and morphologically distinct subdomains, such as rough and smooth membranes and ER exit sites. Despite the structural complexity, the ER is a dynamic organelle, and ER tubules dynamically detach and fuse with each other to form three-way junctions in a microtubule (MT)-dependent fashion (1, 17, 18, 34).

Several proteins have been implicated in the regulation of ER structure. The loss of function of molecules including BNIP1, p97, and p37 involved in ER morphology leads to the loss of three-way junctions; however, the tubular structure of the ER is relatively unaffected (20, 28, 29). Vedrenne and Hauri proposed the mechanisms underlying ER network formation as follows (31): ER membranes are pulled along MTs by MT plus end-directed kinesin-type motor kinesin-1 (8), and the resulting membrane extensions are stabilized by the cytoskeleton-linking ER membrane protein of 63 kDa (13, 30). If ER membranes get close to each other, they fuse in a p97-dependent manner (29). Fusion is further facilitated by the MT-associated p22 that binds to the ER, and thereby ER reticulation is promoted (2). However, the mechanism maintaining the tubular structure of the ER remains unclear.

p31, an ER-localized soluble *N*-ethylmaleimide-sensitive factor attachment protein (SNAP) receptor (SNARE), is a mammalian orthologue of yeast Use1p/Slt1p implicated in Golgi complex-to-ER transport (4, 5, 7). We previously reported that p31 forms a complex with two ER SNAREs, syntaxin 18 (an orthologue of yeast Ufe1p) (11) and BNIP1 (an orthologue of yeast Sec20p) which is involved in the formation of three-way junctions of the ER (20). In yeast, Ufe1p (syntaxin 18) was known to form a complex with Cdc48p, which participates in homotypic ER-ER membrane fusion (16, 23). p31 is a component of the syntaxin 18 complex, where other components are involved in various ER functions, suggesting that p31 also plays various ER functions. Thus, to clarify the biological functions of p31, we generated *p31* knockout mice.

We found that p31 deficiency led to severe disorganiza-

* Corresponding author. Mailing address for Mitsuo Tagaya: School of Life Sciences, Tokyo University of Pharmacy and Life Sciences, 1432-1 Hachioji, Tokyo 192-0392, Japan. Phone: 81-426-76-5419. Fax: 81-426-76-5468. E-mail: tagaya@ls.toyaku.ac.jp. Mailing address for Akihiro Harada: Laboratory of Molecular Traffic, Department of Molecular and Cellular Biology, Institute for Molecular and Cellular Regulation, Gunma University, 3-39-15 Showa, Maebashi, Gunma 371-8512, Japan. Phone: 81-27-220-8840. Fax: 81-27-220-8844. E-mail: aharada@showa.gunma-u.ac.jp.

† These two authors contributed equally to this work.

▽ Published ahead of print on 2 February 2009.

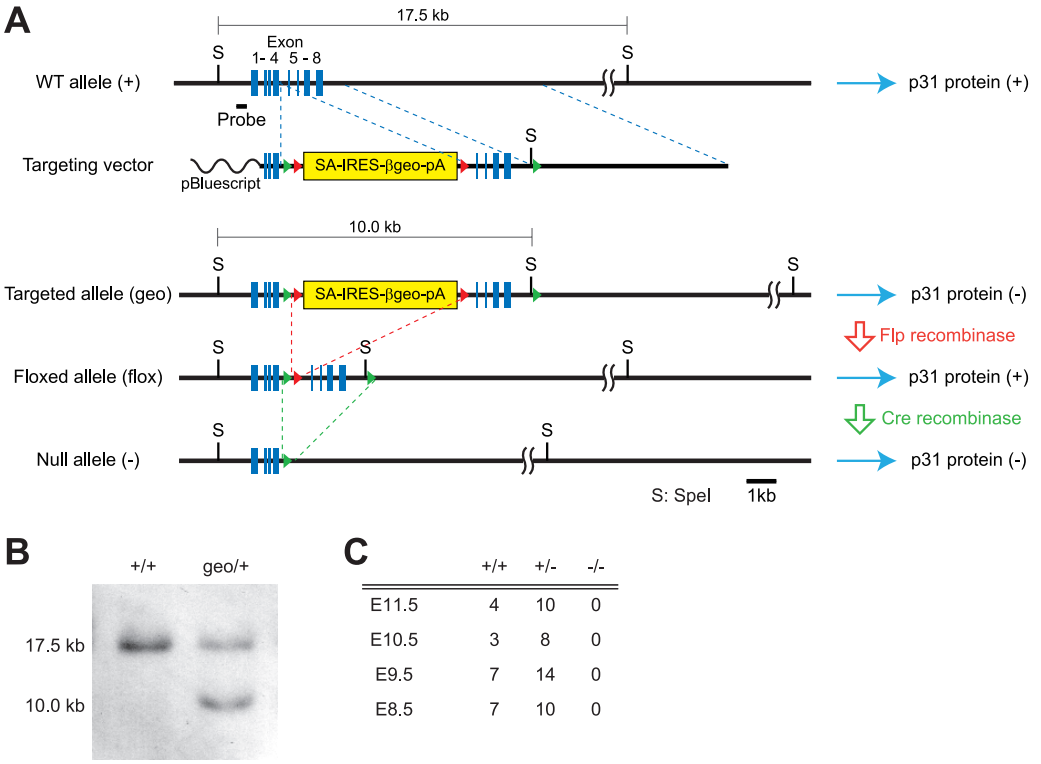

FIG. 1. Construction of *p31* knockout mice. (A) Restriction maps of wild-type (WT) *p31* allele (+), targeting vector, targeted allele (*geo*), floxed allele obtained by crossing with Flp transgenic mice (*flox*), and null *p31* allele (−) obtained after Cre-mediated excision of exons 5 to 8. The wild-type *p31* gene consists of eight coding exons (blue boxes) on chromosome 8. In the targeting vector, two *loxP* sites (green triangles) were introduced into introns flanking exons 5 and 8, and an Flp recombination target (red triangles)-flanked SA-IRES-β-*geo*-poly(A) cassette was inserted between exon 4 and exon 5. In mice with β-*geo* cassettes in both alleles of the target gene (*geo*/*geo*), the transcription of the gene is expected to be interrupted by the strong bcl2 SA and terminated by the poly(A) signal at the end of the cassette. As a result, the expression of the gene is expected to be markedly attenuated. By crossing the *geo*/+ mice with transgenic mice that express Flp recombinase ubiquitously, the SA-IRES-β-*geo*-poly(A) cassette is expected to be excised (*flox*/*flox*), and the expression of the gene will be recovered. We use the resulting *flox*/*flox* mice to generate conditional knockouts by crossing them with Cre transgenic mice. (B) Southern blotting of wild-type (+/+) and recombinant (*geo*/+) ES cells. Genomic DNAs were digested with SpeI and probed with the probe indicated in panel A. (C) Genotypic distribution of embryos from *p31* heterozygous intercrosses.

tion of the ER (vesiculation of and subsequent fusion of the ER structures). The disorganization of the ER retarded the ER-to-Golgi complex transport and accumulation of proteins in the ER, which caused the ER stress response. The ER stress then led to extensive apoptosis. The results of the present study revealed a novel function of p31 in the regulation of ER tubules and prevention of random fusion of ER structures.

MATERIALS AND METHODS

Construction of targeting vector and establishment of the knockout mice. All animal procedures were performed in accordance with the guidelines of the Animal Care and Experimentation Committee of Gunma University, and all animals were bred in the Institute of Animal Experience Research of Gunma University. *p31* knockout mice were generated largely according to the protocols as previously described (24). Briefly, the *p31* gene was isolated from a mouse genomic bacterial artificial chromosome library derived from the 129Sv/J mouse strain (RPCI-22; Children's Hospital Oakland Research Institute). In the targeting vector, an Flp recombination target-flanked splice acceptor (SA)-internal ribosome entry site (IRES)-β-*geo*-poly(A) cassette with an upstream *loxP* site was inserted into intron 4, and a *loxP* site was introduced into intron 8. This construct was used for the generation of $p31^{geo/+}$ mice. To generate tissue-specific knockout mice, we crossed $p31^{geo/+}$ mice with Act-Flp-e transgenic mice (Jackson Laboratory). We then crossed $p31^{flox/+}$ mice with Nestin-Cre transgenic mice or Pcp2-Cre transgenic mice (Jackson Laboratory). To generate nullizygous mice, we crossed $p31^{geo/+}$ mice with cytomegalovirus-Cre transgenic mice (Jackson Laboratory). For genotyping by PCR analysis, the primers used were as follows: Primer 1 (5′-TTAAACCTCAGCACTGAGGAGGCAG-3′), Primer 2 (5′-AGGCAAA GATGACCCTGGGACCTCT-3′), Primer 3 (5′-CCGTACAGTTCCACAAA GGCATCCT-3′), Primer 4 (5′-CCCTTGTACTTGGGACCAACCTCTG-3′), and Primer 5 (5′-ACTAGGGGTTGGAACCTAGATCTGC-3′).

Primers 1 and 2 detected the wild-type allele. Primers 1 and 3 detected the *geo* allele. Primers 4 and 5 detected the null allele.

Cell culture. $p31^{flox/-}$ mice generated by mating between $p31^{floxed/floxed}$ mice and $p31^{+/-}$ mice were dissected on embryonic day 13.5 (E13.5), and mouse embryonic fibroblasts (MEFs) were isolated by trypsinization of embryos. MEFs were cultured in Dulbecco's modified minimal Eagle's medium supplemented with 10% fetal calf serum at 37°C in a humidified 5% CO_2/95% air atmosphere. Adenoviruses were prepared using an adenovirus Cre/LoxP kit version 2.0 (Takara) according to the manufacturer's instructions. Electroporation was carried out using MEF nucleofector kit 1 (Amaxa Biosystems) according to the manufacturer's instructions.

Western blot analyses and immunoprecipitation. Western blot analyses were carried out as described previously (11). To prepare MEF lysates for immunoprecipitation, approximately 80% confluent cells grown on 60-mm dishes were lysed with lysis buffer (20 mM HEPES-KOH, pH 7.2, 150 mM KCl, 2 mM EDTA, 1 mM dithiothreitol, 1% Triton X-100, and protease inhibitor cocktail [Nacalai Tesque]). The lysates were centrifuged in a microcentrifuge at 15,000 rpm for 10 min. The immunoprecipitation experiment was carried out as described previously (11). Western blot analyses for ATF6α, IRE1α, and PERK were carried out as described previously (21).

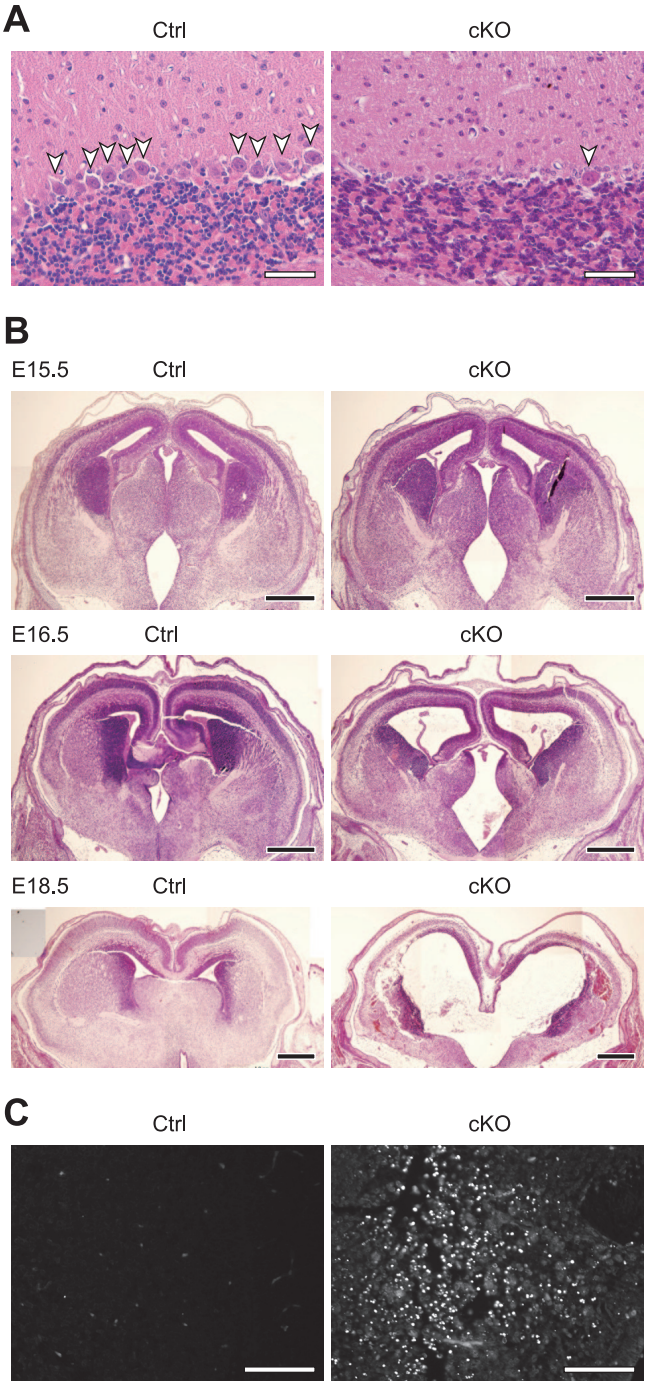

FIG. 2. The *p31* gene is essential for cell viability. (A) Sagittal sections of cerebellum from a 10-week-old control mouse (Ctrl) and a cerebellum-specific knockout mouse (cKO) stained with hematoxylin and eosin. A great reduction in the number of Purkinje cells (arrowheads) was observed in cKO. (B) Coronal sections of E15.5, E16.5, and E18.5 brains from control mice (Ctrl) and CNS-specific knockout mice (cKO) stained with hematoxylin and eosin. (C) Apoptotic cells of E17.5 brains from control mice (Ctrl) and CNS-specific knockout mice (cKO) detected by the TUNEL method. Bars, 50 μm (A), 500 μm (B), and 100 μm (C).

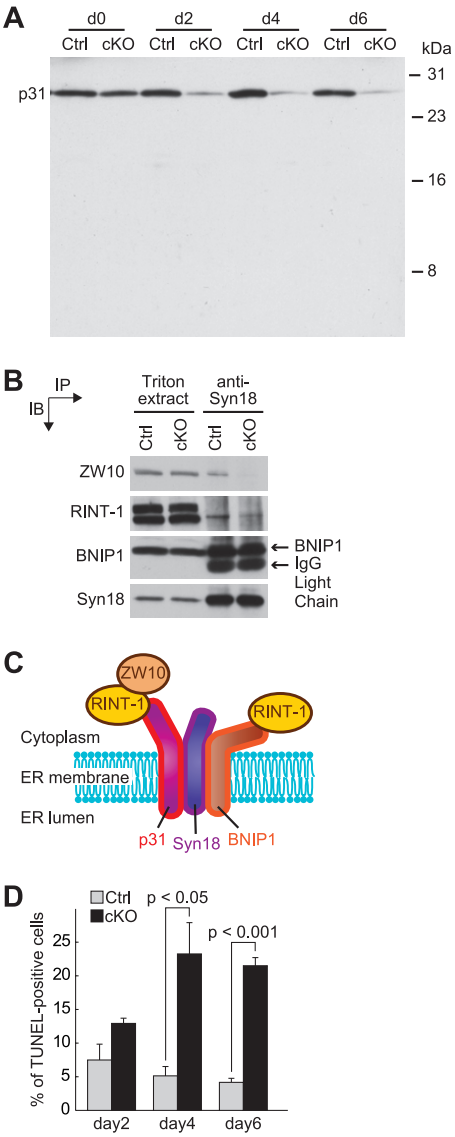

FIG. 3. p31 deletion causes apoptosis in MEFs. (A) Infection of $p31^{flox/-}$ MEFs with Ad-Cre (cKO) progressively decreased p31 expression. $p31^{flox/+}$ MEFs (Ctrl) were infected with Ad-Cre as controls. (B) Association of syntaxin 18 complex components. Triton extracts of $p31^{flox/+}$ (Ctrl) or $p31^{flox/-}$ (cKO) MEFs 2 days after infection with Ad-Cre were subjected to immunoprecipitation (IP) with an anti-syntaxin 18 antibody. The Triton X-100 extracts and the immunoprecipitated proteins were separated and analyzed by immunoblotting (IB) with the indicated antibodies. IgG, immunoglobulin G. (C) p31 forms a complex with two ER SNAREs, syntaxin 18 and BNIP1, and in this large syntaxin 18 complex, p31 forms a subcomplex with ZW10 and RINT-1. (D) $p31^{flox/-}$ MEFs infected with Ad-LacZ (Ctrl) or Ad-Cre (cKO) were fixed at 2, 4, and 6 days after adenovirus treatment, and the percentage of apoptotic cells was determined by the TUNEL method. The percentage of TUNEL-positive cells (mean ± standard error of the mean) was calculated from three independent samples. *P* values were determined by Student's *t* test.

Antibodies and probes. The following antibodies were used: anti-protein disulfide isomerase (anti-PDI) (Stressgen), anti-BiP (Affinity BioReagents), anti-green fluorescent protein (anti-GFP) (Nacalai Tesque), anti-CHOP (Santa Cruz Biotechnology), fluorescein isothiocyanate-labeled anti-α-tubulin (Sigma), anti-GS28 (BD Transduction Laboratories), anti-LAMP2 (clone Abl 93; Developmental Studies Hybridoma Bank), anti-Ire1α (Cell Signaling Technology), anti-PERK (Rockland), and anti-Sec13 (a gift from W. Hong, Institute of Molecular and Cell Biology, Singapore). Polyclonal antibodies against p31, BNIP1, ZW10, RINT-1, Bap31, and a monoclonal anti-syntaxin

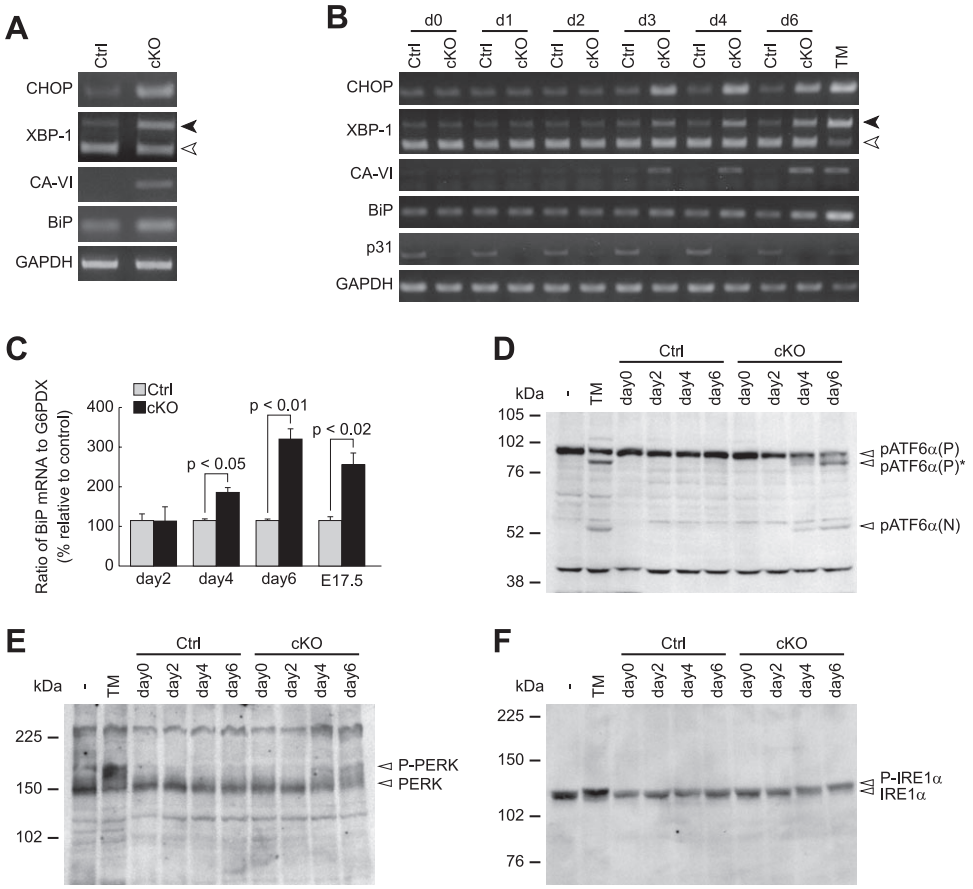

FIG. 4. p31 deletion leads to ER stress. (A and B) RT-PCR analysis of ER stress-associated molecules in brains (A) and MEFs (B). Black and white arrowheads indicate spliced and unspliced forms of XBP-1, respectively. GAPDH was used as an internal control. (A) RT-PCR analysis of E17.5 brains from control mice (Ctrl) and CNS-specific knockout mice (cKO). (B) RT-PCR analysis of $p31^{flox/+}$ (Ctrl) or $p31^{flox/-}$ (cKO) MEFs infected with Ad-Cre. "dX" represents samples prepared on day X after adenovirus treatment. As a positive control, MEFs were treated with tunicamycin for 24 h (TM). (C) Quantitative RT-PCR to evaluate level of BiP mRNA showed increased expression in p31-deficient MEFs (days 2, 4, and 6) and embryonic brains (E17.5). The ratio of BiP mRNA to G6PDX (glucose 6-phosphate dehydrogenase X-linked) calculated from three independent samples, were normalized against data of control. *P* values were determined by Student's *t* test. (D to F) Western blot analyses showed increased cleavage of ATF6α (D) and increased phosphorylation of PERK (E) and IREα (F). pATF6α(P), pATF6α(P)*, and pATF6α(N) indicate full-length ATF6α, nonglycosylated full-length ATF6α, and cleaved form of ATF6α, respectively.

18 antibody were raised as described previously (11, 20, 32). ATF6α antibody was raised as described previously (10).

TUNEL staining. Terminal deoxynucleotidyltransferase-mediated dUTP nick end labeling (TUNEL) staining was performed using an in situ death detection kit (Roche) according to the manufacturer's instructions.

Histological analysis. Immunofluorescence microscopy was performed as described previously (24). Electron microscopy was also performed as described previously (24, 35).

RNA isolation and reverse transcription-PCR (RT-PCR). Total RNA was extracted from cultured cells and brains from embryos by a phenol-chloroform extraction procedure using RNAiso (Takara). Three micrograms of total RNA was primed with oligo(dT) to synthesize first-strand cDNA with reverse transcriptase. The primers used for PCR were as follows: p31 sense primer (5′-CAC GTTACACCAGTGAGATG-3′), p31 antisense primer (5′-AGGTGTGCAGG CTTTCTTGT-3′), GAPDH (glyceraldehyde-3-phosphate dehydrogenase) sense primer (5′-ACCACAGTCCATGCCATCAC-3′), and GAPDH antisense primer (5′-TCCACCACCCTGTTGCTGTA-3′).

RT-PCR analysis was performed as described for CHOP and BiP (26), for CA-VI (25), and for the spliced form of XBP-1 (6). Quantitative RT-PCR was performed as described previously (24). To evaluate the mRNA levels of BiP, we used Universal ProbeLibrary (Roche). Probe number 64 for BiP and probe number 78 for glucose 6-phospate dehydrogenase X-linked (G6PDX) were obtained. The primers used for quantitative RT-PCR were as follows: BiP sense primer (5′-AACCCCGATGAGGCTGTAG-3′), BiP antisense primer (5′-CAT CAAGCGGTACCAGATCA-3′), G6PDX sense primer (5′-GAAAGCAGAGT GAGCCCTTC-3′), and G6PDX antisense primer (5′-CATAGGAATTACGG GCAAAGA-3′).

Protein transport from the ER to the Golgi complex. MEFs were infected with an adenovirus encoding tsO45-vesicular stomatitis virus-encoded glycoprotein fused with green fluorescent protein (VSVG-GFP) or MDR1 fused with GFP (MDR1-GFP). The cells infected with Ad-VSVG-GFP were incubated at 40°C for 20 h and then shifted to 37°C to allow transport from the ER to the Golgi complex. The cells infected with Ad-MDR1-GFP were incubated at 37°C for 12 h and washed with phosphate-buffered saline to remove adenoviruses, and then they were incubated at 37°C for 12 h. The cells were fixed and processed for immunofluorescence analysis. The biochemical transport assay was carried out as described previously (11).

RESULTS

p31 is an essential molecule for cell viability. To generate *p31* conditional knockout mice, we used a revertible knockout system as described previously (24) (Fig. 1A and B). First, we analyzed conventional knockout mice that lack *p31* in the whole body ($p31^{geo/geo}$ and $p31^{-/-}$). Conventional knockout mice showed early embryonic lethality before E8.5 (Fig. 1C). We therefore sought to generate tissue-specific knockout mice

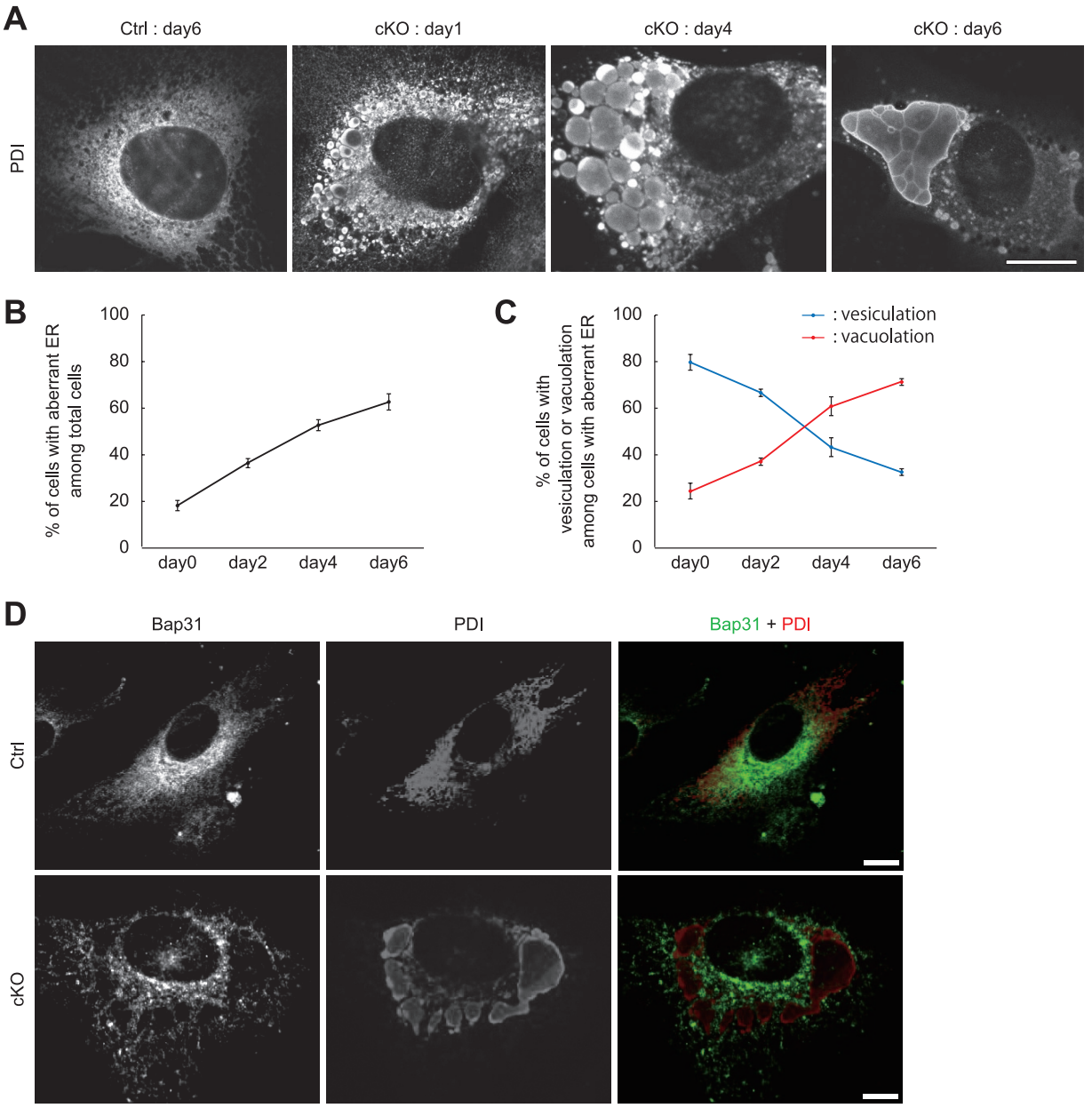

FIG. 5. p31 deletion causes vesiculation and fusion of the ER. (A) $p31^{flox/+}$ (Ctrl) or $p31^{flox/-}$ (cKO) MEFs infected with Ad-Cre were stained with the antibody against PDI. The ER vesiculates at 1 day after Ad-Cre treatment. The vesiculated ER grows larger to form large vacuoles with time. (B) Cells with aberrant ER (vesiculation and vacuolation) among total cells were already observed 0 days after Ad-Cre treatment and increased with time. The error bars represent the mean ± the standard deviation (SD) ($n = 3$). (C) p31 deficiency caused ER vesiculation followed by ER vacuolation. The percentage of cells with vesiculated or vacuolated ER membranes (mean ± SD) was calculated from three independent samples. (D) $p31^{flox/+}$ (Ctrl) or $p31^{flox/-}$ (cKO) MEFs infected with Ad-Cre were double stained with antibodies against Bap31 (green) and PDI (red) 6 days after adenovirus treatment. Bar, 10 μm.

to determine the role of p31. To this end, $p31^{flox/flox}$ mice were generated by intercrossing between $p31^{flox/+}$ mice that had been obtained by mating $p31^{geo/+}$ mice with transgenic mice expressing Flp recombinase. $p31^{flox/flox}$ mice were born at Mendelian frequency and were indistinguishable from wild-type mice (data not shown). By breeding $p31^{flox/flox}$ or $p31^{flox/-}$ mice with transgenic mice expressing Cre recombinase under the control of the Pcp2 promoter (*Pcp2-cre*) and nestin promoter (*Nestin-cre*), we generated Purkinje cell-specific and central nervous system (CNS)-specific conditional knockout mice, respectively.

Mice lacking *p31* in Purkinje cells ($p31^{flox/-}$; *Pcp2-cre*) displayed cerebellar ataxia, such as abnormal gait, after 10 weeks postnatal. Hematoxylin and eosin staining of the cerebellum showed a significant decrease in the number of Purkinje cells (Fig. 2A). CNS-specific knockout mice ($p31^{flox/flox}$; *Nestin-cre*) died within 1 day of birth, although the knockout was not lethal during embryogenesis (data not shown). Marked changes in

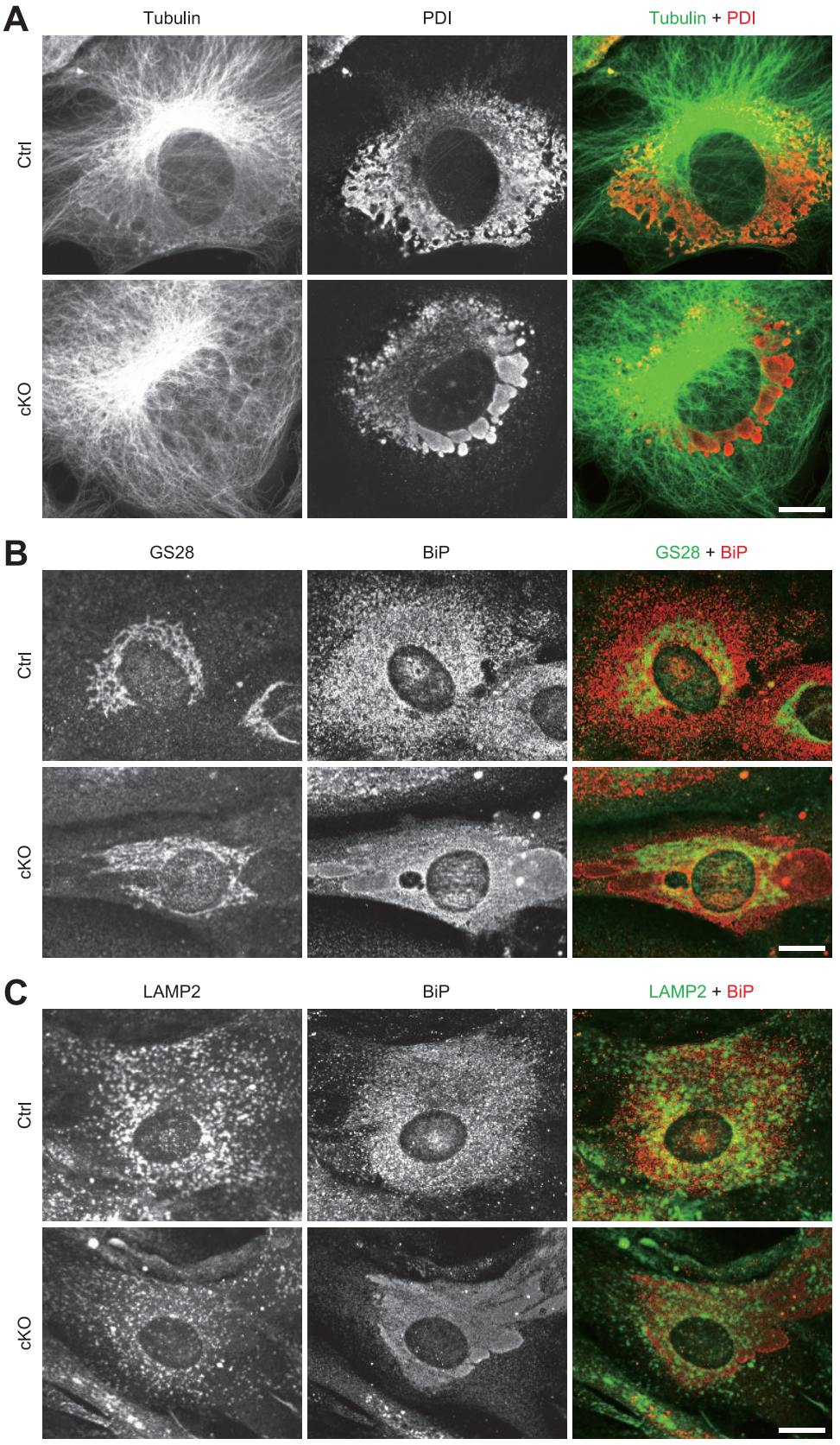

FIG. 6. ER aberration neither results from MT disruption nor results in apparent disruption of the Golgi complex and lysosome. $p31^{flox/+}$ (Ctrl) or $p31^{flox/-}$ (cKO) MEFs infected with Ad-Cre were double stained with antibodies against tubulin (green) and PDI (red) (A), GS28 (green) and BiP (red) (B), and LAMP2 (green) and BiP (red) (C) 6 days after adenovirus treatment. Bars, 10 μm.

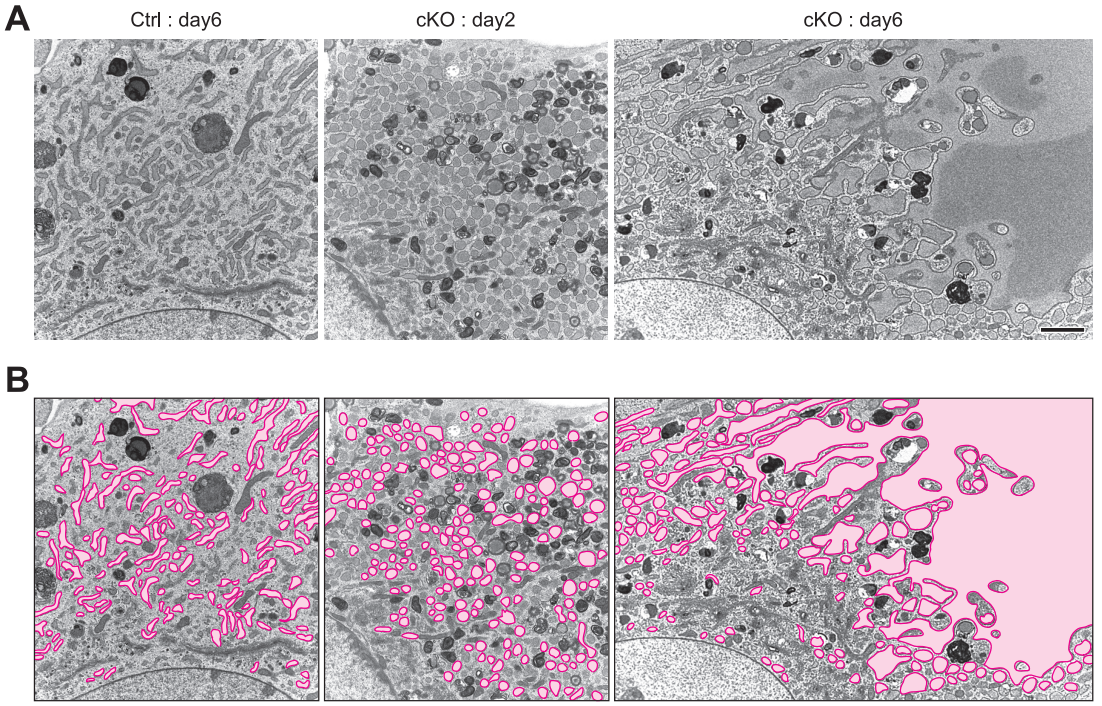

FIG. 7. ER structure in p31-deficient MEFs. (A) Electron microscopic analysis of $p31^{flox/-}$ MEFs infected with Ad-LacZ (Ctrl) or Ad-Cre (cKO) was performed 2 or 6 days after adenovirus treatment. The lumen of the ER markedly dilated 6 days after p31 depletion, whereas no change was observed in the control MEFs. Bar, 2 μm. (B) The same images as those shown in panel A, except that the ERs were labeled with pseudocolor.

brain architecture, such as dilated ventricles and a decrease in the thickness of the cerebral cortices, were observed in the embryonic brain (Fig. 2B). To clarify the cause of this phenotype, we performed TUNEL staining. As shown in Fig. 2C, a large number of apoptotic cells were observed in the brains of the $p31^{flox/flox}$; *Nestin-cre* mice, suggesting that apoptosis is the cause of the abnormal brain morphology.

p31 deficiency caused ER stress. To confirm the essentiality of the *p31* gene, we deleted *p31* in $p31^{flox/-}$ MEFs using an adenovirus encoding Cre recombinase (Ad-Cre). Immunoblotting revealed that the expression of p31 remarkably decreased 2 days after Ad-Cre treatment (Fig. 3A). On the other hand, the expression of other syntaxin 18 complex components, such as syntaxin 18, BNIP1, ZW10, and RINT-1, were unchanged in Ad-Cre-treated cells (Fig. 3B).

We previously demonstrated that p31 forms a subcomplex with ZW10 and RINT-1 in a large syntaxin 18 complex as illustrated in Fig. 3C (11). Consistent with this, p31 deficiency caused dissociation of ZW10 and partial dissociation of RINT-1 from syntaxin 18 (Fig. 3B). The incomplete dissociation of RINT-1 from syntaxin 18 may be attributed to the interaction of RINT-1 with BNIP1, another syntaxin 18-associated SNARE (20).

Similar to neurons in CNS-specific *p31* knockout, the number of TUNEL-positive cells was larger in $p31^{flox/-}$ MEFs infected with Ad-Cre than that in $p31^{flox/-}$ MEFs infected with a control adenovirus encoding LacZ (Ad-LacZ), indicating the occurrence of apoptosis in these cells (Fig. 3D). To understand the mechanism by which apoptosis is induced in p31-deficient cells, we examined whether ER stress was induced by p31 depletion. We investigated the expression levels of ER stress-associated molecules (CHOP/GADD153, the spliced form of XBP-1, CA-VI [type B], BiP) (9, 12, 22). RT-PCR analysis revealed that the expression levels of these molecules were upregulated in *p31*-deficient brains (Fig. 4A and C) and MEFs (Fig. 4B and C).

Under ER stress, two ER stress sensors, PERK and IRE1, are known to be phosphorylated, and another ER stress sensor, ATF6, is cleaved. In p31-deficient MEFs, we observed increased cleavage of ATF6α and increased phosphorylation of PERK and IRE1α (Fig. 4D to F), further confirming that p31 deficiency caused ER stress.

p31 regulates the ER morphology in MEFs. Next, we investigated the ER morphology in *p31*-deficient MEFs by immunofluorescence microscopy using an antibody against a lumenal ER protein, PDI. At an early stage of p31 depletion, the majority of the cells showed vesiculated ER structures, and as time progressed, the percentage of the cells with vacuolated ER structures increased, whereas that of the cells with vesiculated ER structures decreased (Fig. 5A to C), suggesting the fusion of the ER vesicles. No change in ER morphology was observed in $p31^{flox/+}$ MEFs infected with Ad-Cre or in $p31^{flox/-}$ MEFs infected with Ad-LacZ (data not shown), ruling out the possibility that this morphological change of the ER was due to adenovirus infection.

To determine whether the aberrant staining pattern of PDI reflects aggregation of PDI within the ER or a change in the ER structure itself, we used Bap31 as a marker of the ER membrane. As shown in Fig. 5D, Bap31 was located on the membranes of vacuolated structures stained by anti-PDI antibody, suggesting that p31 deficiency caused the swelling of ER membrane.

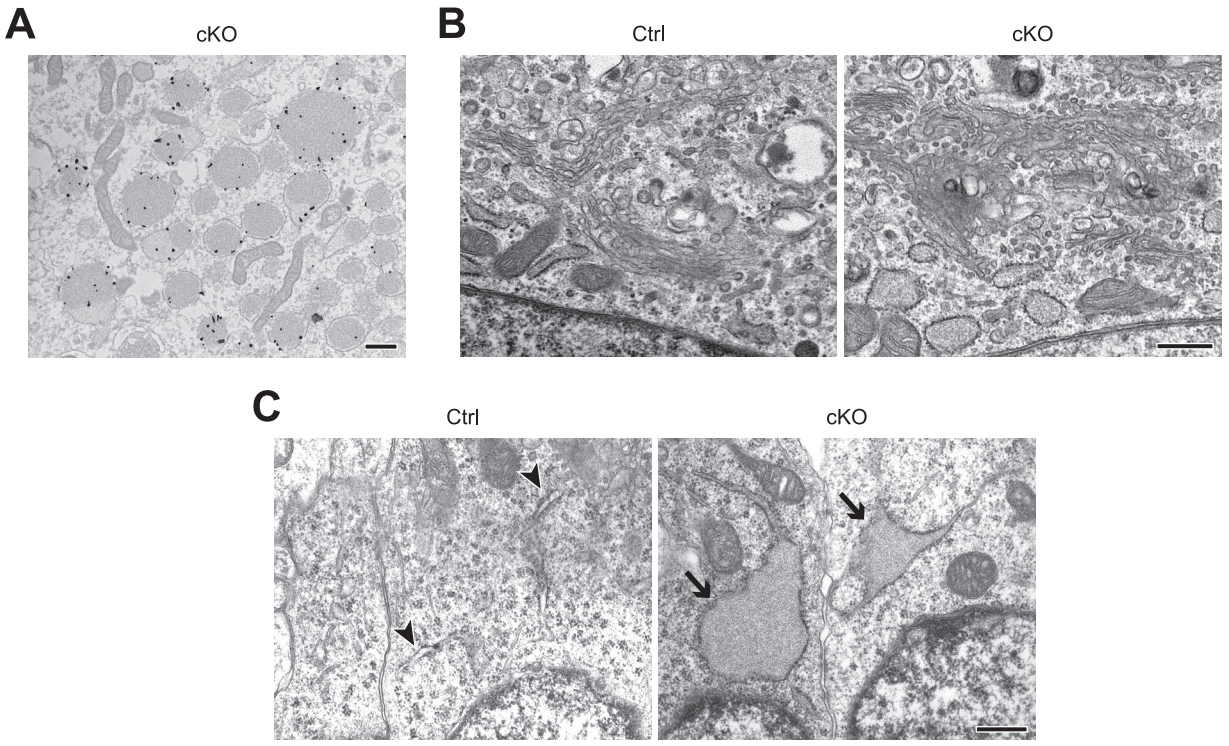

FIG. 8. Characterization of abnormal ERs by electron microscopy. (A) Immunogold labeling of PDI was found in the vesiculated ER of p31-deficient MEFs. $p31^{flox/-}$ MEFs infected with Ad-Cre were observed 6 days after adenovirus treatment. (B) The Golgi complex is not disrupted in p31-deficient MEFs. $p31^{flox/-}$ MEFs infected with Ad-LacZ (Ctrl) or Ad-Cre (cKO) were observed 6 days after adenovirus treatment. (C) Enlargement of ERs (arrows) was also observed in neurons from the E16.5 brains of CNS-specific knockout mice (cKO) but not in neurons of control mice (Ctrl). Normal ERs are indicated by arrowheads. Bars, 500 nm.

The ER is linked to MTs with various proteins; thus, we sought to investigate MT organization and the relationship between MTs and the aberrant ER. The organization of MTs is similar between p31-deficient cells and control cells, indicating that ER aberration does not result from MT disruption (Fig. 6A).

To investigate the effects of p31 deficiency on the morphologies of the Golgi complex and lysosome, we stained MEFs with antibodies against GS28 or LAMP2. The staining patterns of GS28 and LAMP2 were relatively unchanged in cells with an abnormal ER (Fig. 6B and C).

Electron microscopic analysis showed an abnormal ER structure in p31-deificient MEFs and brains. To analyze the intracellular membrane structures in more detail, we carried out electron microscopy. We observed numerous small and round ERs at an early stage of p31 depletion (2 days after adenovirus treatment), and ER "vesicles" became significantly larger and fewer at the late stage of p31 depletion (6 days after

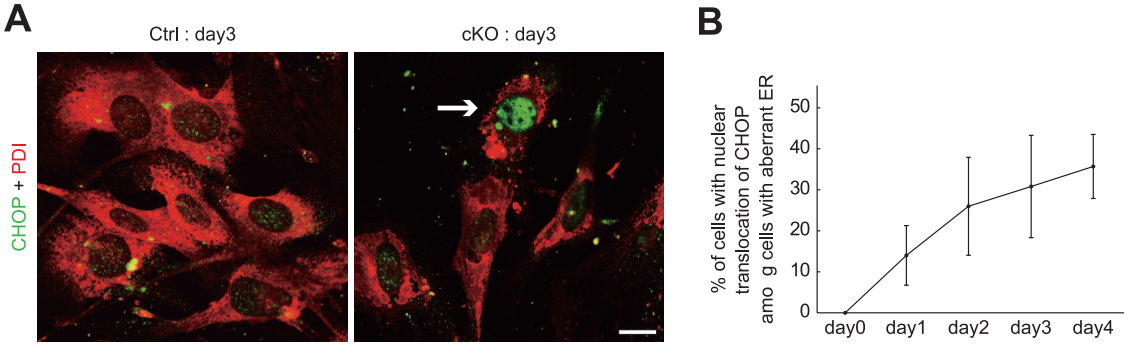

FIG. 9. Disorganization of the ER caused by p31 deficiency led to ER stress response. (A) $p31^{flox/+}$ (Ctrl) or $p31^{flox/-}$ (cKO) MEFs infected with Ad-Cre were double stained with antibodies against PDI (red) and CHOP (green). "day3" represents, e.g., samples prepared on day 3 after adenovirus treatment. The arrow indicates a cell with nuclear translocation of CHOP. (B) The ratio of the number of cells showing nuclear translocation of CHOP versus the number of cells showing the aberrant staining pattern of PDI increased in a time-dependent manner in p31-deficient cells. Note that no CHOP nuclear staining was observed at day 0 after Ad-Cre treatment when aberrant ER was already observed. The error bars represent the mean ± the standard error of the mean ($n = 3$). Bar, 10 μm (A).

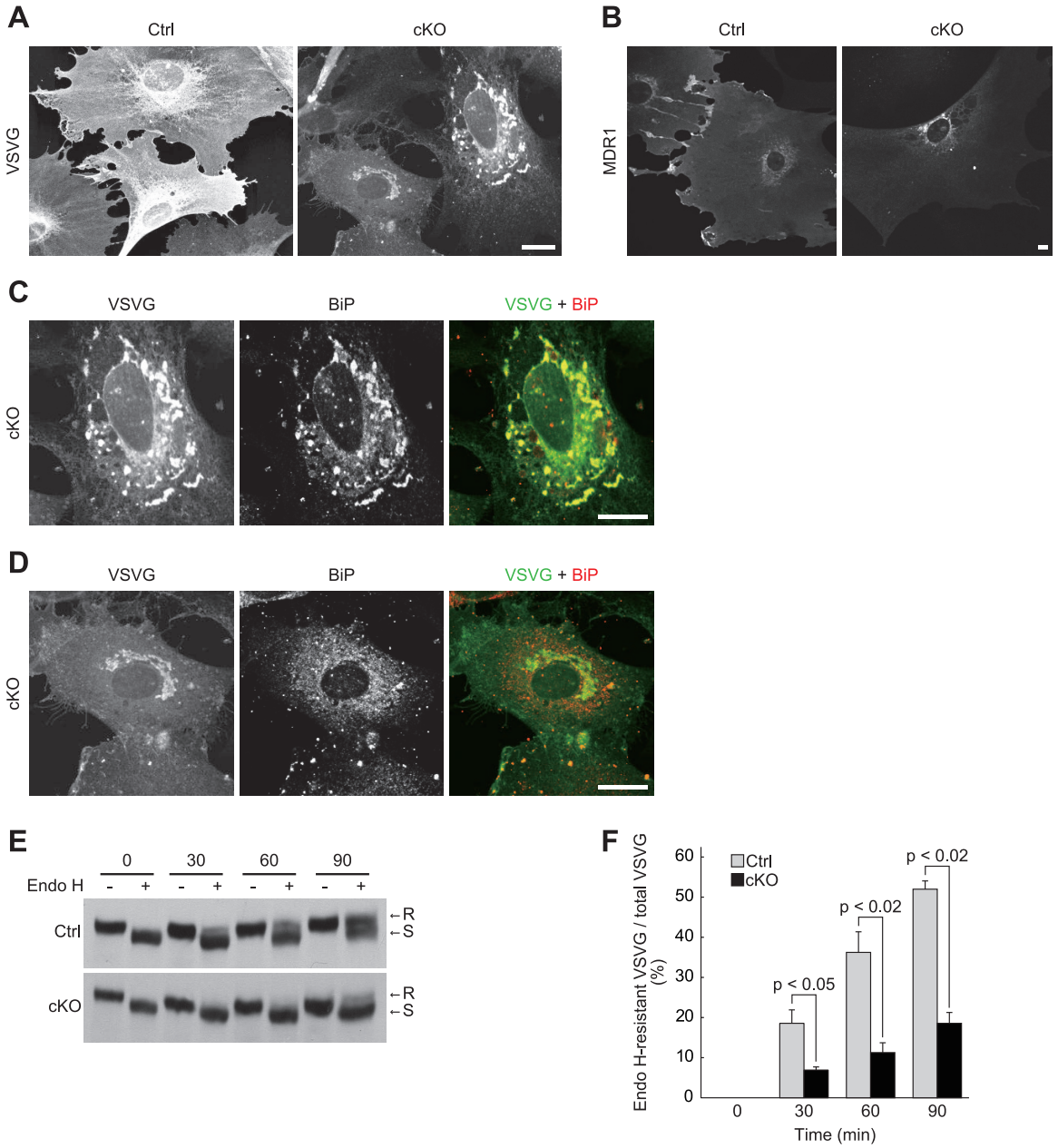

FIG. 10. ER-to-Golgi complex protein transport is impaired in p31-deficient MEFs. (A, C, and D) $p31^{flox/-}$ MEFs were infected with Ad-LacZ (Ctrl) or Ad-Cre (cKO), followed by infection with another adenovirus encoding VSVG-GFP. Four days after the first adenovirus treatment, they were fixed 60 min after a temperature shift to a permissive temperature and double stained with anti-GFP and anti-BiP antibodies. The distribution of VSVG, which is detected by staining with the anti-GFP antibody, is shown in panel A. (C and D) Double-stained images of two cells in panel A (cKO) at higher magnification. (B) $p31^{flox/+}$ (Ctrl) or $p31^{flox/-}$ (cKO) MEFs infected with Ad-Cre were infected with adenovirus encoding MDR1-GFP and were stained using anti-GFP antibody. (A to D) Bars, 10 μm. (E and F) VSVG-expressing control MEFs (Ctrl) and p31-deficient MEFs (cKO) were treated as described above, except that the cells were lysed, subjected to Endo H treatment, and analyzed by immunoblotting with a polyclonal anti-VSVG antibody. A representative experiment is shown in panel E. R and S denote Endo H-resistant and Endo H-sensitive forms of VSVG, respectively. (F) Ratio of Endo H-resistant VSVG to total VSVG (mean ± standard error of the mean) calculated from three independent samples. *P* values were determined by Student's *t* test.

adenovirus treatment) (Fig. 7). Immunoelectron microscopic analysis using an anti-PDI antibody unequivocally demonstrated that vesiculated membranes are derived from the ER (Fig. 8A). In contrast to the significant morphological change of the ER, the shape of the Golgi complex in p31-deficient cells was similar to that of control cells (Fig. 8B). To confirm whether p31 deficiency changes ER morphology in vivo, we next investigated ER morphology in neurons of CNS-specific knockout mice. We observed enlargement of the ER in p31-deficient neurons as observed in p31-deficient MEFs (Fig. 8C). These observations suggest that p31 is a molecule involved in the maintenance of the ER structure and that the aberrant ER

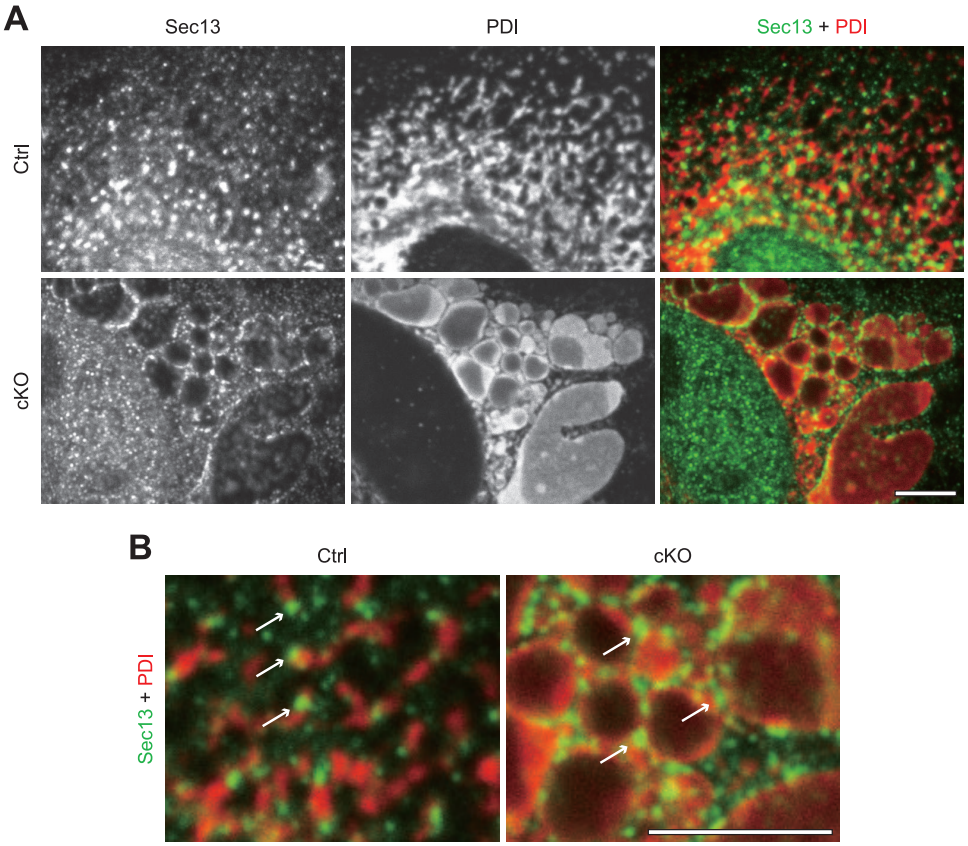

FIG. 11. ER exit sites are not disrupted in the enlarged ER. (A) $p31^{flox/-}$ MEFs infected with Ad-LacZ (Ctrl) or Ad-Cre (cKO) were fixed 4 days after adenovirus treatment and double stained with antibodies against Sec13 (green) and PDI (red). (B) Higher-magnification images of merged images in panel A. Arrows indicate punctate localization of Sec13 along the ER, demonstrating that ER exit sites are not disrupted in p31-deficient MEFs. (A and B) Bars, 5 μm.

morphology caused by the lack of *p31* is likely to lead to neuronal death in CNS-specific knockout mice.

The disorganization of the ER caused by p31 deficiency led to ER stress response. Under ER stress, a transcription factor, CHOP, is upregulated and translocates to the nucleus to activate transcription of apoptosis-inducing machinery (33). CHOP accumulated in the nucleus in MEFs upon p31 depletion (Fig. 9A). To determine the temporal relationship between nuclear translocation of CHOP and the change in ER morphology, we double-stained MEFs with antibodies against CHOP and PDI at various times after p31 deletion. As shown in Fig. 9B and Fig. 5B, the percentage of cells with nuclear translocation of CHOP among cells with aberrant ER increased with time. This indicates that the morphological change of the ER preceded nuclear translocation of CHOP, suggesting that this change in ER morphology results in ER stress.

An abnormal morphology of the ER caused by p31 deficiency-impaired protein transport from the ER to the Golgi complex. Because of the marked morphological change of the ER in p31-deficient MEFs, protein transport from the ER to the Golgi complex may be affected. To test this possibility, we examined the transport of VSVG-GFP. In control cells, VSVG-GFP was transported from the ER to the Golgi complex and then to the plasma membrane, resulting in a broad staining of the plasma membrane 60 min after a temperature shift to a permissive temperature (Fig. 10A). In p31-deficient MEFs, a large fraction of VSVG-GFP was detected in the ER with an abnormal morphology, and it was detected only faintly on the plasma membrane, indicating that VSVG-GFP transport from the ER to the Golgi complex was impaired in p31-deficient MEFs. A similar result was obtained when we examined the ER-to-Golgi complex transport of multidrug resistance protein 1 (MDR1-GFP) (Fig. 10B).

In p31-deficient MEFs, the amount of VSVG-GFP transported from the ER to the Golgi complex and plasma membrane appeared to roughly correlate with the extent of the intact ER; that is, the more disorganized the ER, the less VSVG-GFP was on the plasma membrane (compare Fig. 10C with D). Therefore, the disorganized ER structure may cause inefficient ER-to-Golgi complex protein translocation, which results in the delayed transport of VSVG-GFP from the ER to the plasma membrane.

To biochemically confirm that VSVG-GFP was retained in the ER, we examined the endoglycosidase H (Endo H) sensitivity of VSVG-GFP. If VSVG-GFP is transported to the Golgi complex, it acquires Endo H resistance. The ratio of the Endo H-resistant form to total VSVG in p31-deficient MEFs was less than half that in $p31^{flox/+}$ MEFs infected with Ad-Cre (Fig. 10E and F).

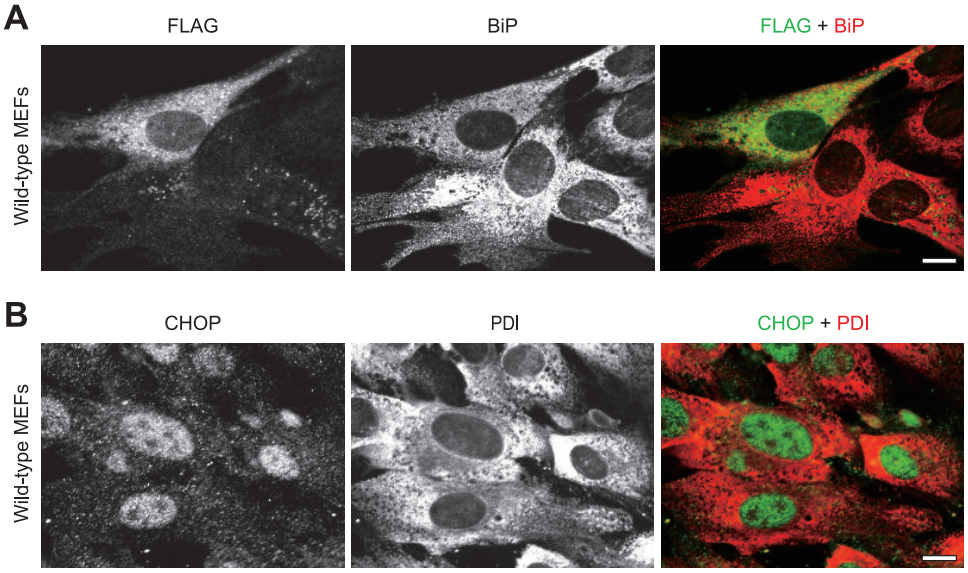

FIG. 12. The blockade of ER-Golgi complex transport and tunicamycin treatment do not cause ER vesiculation. (A) Overexpression of a dominant negative form of Sar1 (Sar1[T39N]) in wild-type MEFs showed no effect on ER structure, suggesting that ER vesiculation was not due to impaired ER-to-Golgi complex transport. Wild-type MEFs were electroporated with FLAG-Sar1[T39N], and after 24 h, they were fixed and double stained with antibodies against FLAG (green) and BiP (red). (B) Tunicamycin treatment showed no effect on ER structure in wild-type MEFs, suggesting that ER vesiculation was not due to ER stress. Wild-type MEFs were treated with 10 μg/ml tunicamycin for 12 h, and they were fixed and double stained with antibodies against CHOP (green) and PDI (red). (A and B) Bars, 10 μm.

One possible explanation for the partial impairment of VSVG-GFP transport in p31-deficient cells is that ER exit sites, which are responsible for protein export from the ER (15), are disorganized as a consequence of ER vesiculation. To explore this possibility, we stained MEFs using an antibody against Sec13, which is a marker of ER exit sites (27). As shown in Fig. 11A and B, punctate Sec13 localization, similar to that in control cells, was still observed in p31-deficient MEFs, ruling out the possibility that the disorganization of ER exit sites caused the impairment of VSVG-GFP transport in p31-deficient cells.

To further exclude the possibility that the impaired protein transport from the ER to the Golgi complex induces the disorganization of the ER in p31-deficient MEFs, we blocked protein transport from the ER using a dominant negative form of Sar1 (Sar1[T39N]) (14) in wild-type MEFs and observed the effect on ER structure. Overexpression of Flag-tagged Sar1[T39N] showed no obvious effect on the ER structure (Fig. 12A), suggesting that ER vesiculation was not due to an impaired transport between the ER and the Golgi complex.

To rule out the possibility that ER stress causes the disorganization of ER structure in p31-deficient cells, we treated wild-type MEFs with tunicamycin, an inducer of ER stress. In cells with nuclear translocation of CHOP, we could not observe vesiculation and enlargement of the ER as observed in p31-deficient cells (Fig. 12B), suggesting that ER disorganization was not due to ER stress response.

DISCUSSION

The present study demonstrated that p31 is required for the maintenance of the ER tubular structure (Fig. 13). We also showed that p31 is essential for cell survival as in the case of its yeast orthologue Use1p/Slt1p (4, 5, 7); however, the role of Use1p/Slt1p in the regulation of ER morphology has not yet been shown.

ER morphological changes induced by p31 deficiency. We found that the lack of *p31* induced marked morphological changes in the ER both in vivo (neurons) and in vitro (MEFs). Previous studies showed that the loss of function of molecules involved in ER morphological regulation, such as BNIP1, p97, and p37, leads to the loss of three-way junctions of ER tubules (20, 28, 29). However, the tubular structure of the ER was relatively unaffected. In contrast to these previous findings, our study showed that p31 deficiency disrupted the tubular structure itself, resulting in the formation of vesicles and large ER-derived vacuolar structures. This type of extensive structural changes in the ER tubules has not been demonstrated to date.

Although ER-to-Golgi complex protein transport was partly impaired in cells with an abnormal morphology of the ER (Fig. 10), this is not the reason for the disorganization of ER structure because blockade of ER-to-Golgi complex transport by a dominant-negative Sar1 did not affect the ER structure (Fig. 12A). Also, in cells treated with tunicamycin, we observed no effects on ER morphology, ruling out the possibility that ER stress was the cause of ER disruption (Fig. 12B). These results suggest that p31 has a direct role in maintaining the organization of ER tubules.

Two steps are suggested: vesiculation and fusion. We demonstrated that multiple steps were required for the formation or maintenance of the ER tubules, which has not been described so far. In the absence of p31, we found that the ER is disrupted in two steps: vesiculation and subsequent enlargement (probably by fusion). This suggests that p31 is required

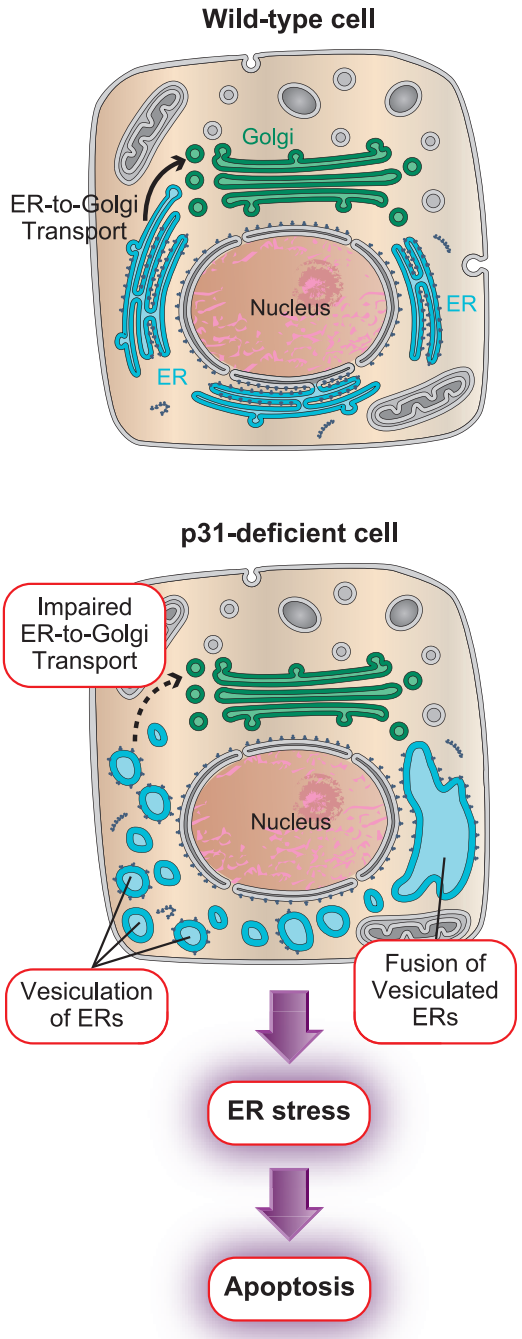

FIG. 13. Schematic diagram showing changes in p31-deficient cells. In p31-deficient cells, a two-stage change in ER structure was observed; vesiculation and subsequent enlargement (fusion) of vesiculated membranes. Thus, the tubular structure of the ER was completely disorganized. This suggests that p31 is involved in the maintenance of ER tubules and prevention of random fusion of ER structures. The disorganized ER structure causes inefficient ER-to-Golgi complex protein transport, which results in ER stress-induced apoptosis. The ER and Golgi complex are blue and green, respectively.

for the maintenance of ER tubules as well as the prevention of homotypic fusion between ER structures.

p31 is a component of the syntaxin 18 complex, which mediates the homotypic fusion of the ER. We have previously shown that p31 forms a complex with syntaxin 18 and BNIP1 (11, 20). We showed that p31 deficiency caused no effects on the interaction between syntaxin 18 and BNIP1 in cells (Fig. 3B) and in an in vitro system (3). Taken together, these results show that another component(s) in the syntaxin 18 complex might be involved in the homotypic fusion of the ER and that p31 seems to be a negative regulator of homotypic fusion of the ER because p31 deficiency caused enlargement of the ER membrane following vesiculation of the ER. Considering the multiple putative functions of p31 regarding the morphology of the ER, identification of molecules that interact with p31 will greatly increase our knowledge of the molecular mechanisms underlying the formation of the ER in the future.

Disruption of ER morphology leads to apoptosis. In this present study, we showed a pathway of apoptosis that is induced by perturbation of ER morphology. We demonstrated that an extreme morphological change in the ER leads to a reduced efficiency in ER-to-Golgi complex transport. This reduced efficiency in ER-to-Golgi complex transport leads to the accumulation of proteins in the ER, which then leads to an ER stress response, subsequent accumulation of CHOP in the nucleus, and, finally, cell death.

ER stress has been suggested to be involved in some human neurodegenerative disorders, such as Parkinson's disease and Alzheimer's disease, as well as other disorders such as diabetes (12, 19, 36). However, the key mechanisms underlying these disorders have been thought to be aggregation of unfolded proteins within cells. The present report presented an additional mechanism of ER stress-induced cell death, suggesting the possibility that this pathway might be involved in cell death in other types of degenerative disease.

ACKNOWLEDGMENTS

We thank Mutsumi Takano, Tomoko Horie, Yumiko Okada, Chihiro Ohsawa, and Makiko Kanesawa for help with cell culture, animal care, and microscopy; Fumihiro Sugiyama and Satoru Takahashi for generating chimeric mice; Ken Sato, Miyuki Sato, Masahiro Nagasawa, Itaru Kojima, Chihiro Mogi, and Fumikazu Okajima for instructions on various techniques; Wanjin Hong for the antibody; Yasumasa Ishida for providing the construct; and Kohei Arasaki and Hidenori Hirose for helpful comments at the start of this work.

This work was supported by grants-in-aid, the 21st Century Center of Excellence Program, the Global Center of Excellence Program, Initiatives for Attractive Education in Graduate Schools from the Japanese Ministry of Education, Culture, Sports, Science, and Technology, The Uehara Memorial Foundation to A.H., the Takeda Science Foundation to T.S. and A.H., The Nakajima Foundation to T.S., and The Cell Science Research Foundation to A.H.

REFERENCES

1. **Allan, V. J., and R. D. Vale.** 1991. Cell cycle control of microtubule-based membrane transport and tubule formation in vitro. J. Cell Biol. **113:**347–359.
2. **Andrade, J., H. Zhao, B. Titus, S. Timm, and M. Barroso.** 2004. The EF-hand $Ca2^{+}$-binding protein p22 plays a role in microtubule and endoplasmic reticulum organization and dynamics with distinct $Ca2^{+}$-binding requirements. Mol. Biol. Cell **15:**481–496.
3. **Aoki, T., M. Kojima, K. Tani, and M. Tagaya.** 2008. Sec22b-dependent assembly of endoplasmic reticulum Q-SNARE proteins. Biochem. J. **410:** 93–100.
4. **Belgareh-Touzé, N., M. Corral-Debrinski, H. Launhardt, J. M. Galan, T. Munder, S. Le Panse, and R. Haguenauer-Tsapis.** 2003. Yeast functional analysis: identification of two essential genes involved in ER to Golgi trafficking. Traffic **4:**607–617.
5. **Burri, L., O. Varlamov, C. A. Doege, K. Hofmann, T. Beilhartz, J. E. Rothman, T. H. Söllner, and T. Lithgow.** 2003. A SNARE required for retrograde transport to the endoplasmic reticulum. Proc. Natl. Acad. Sci. USA **100:** 9873–9877.

6. **Calfon, M., H. Zeng, F. Urano, J. H. Till, S. R. Hubbard, H. P. Harding, S. G. Clark, and D. Ron.** 2002. IRE1 couples endoplasmic reticulum load to secretory capacity by processing the XBP-1 mRNA. Nature **415:**92–96.
7. **Dilcher, M., B. Veith, S. Chidambaram, E. Hartman, H. D. Schmitt, and G. Fischer von Mollard.** 2003. Use1p is a yeast SNARE protein required for retrograde traffic to the ER. EMBO J. **22:**3664–3674.
8. **Feiguin, F., A. Ferreira, K. S. Kosik, and A. Caceres.** 1994. Kinesin-mediated organelle translocation revealed by specific cellular manipulations. J. Cell Biol. **127:**1021–1039.
9. **Groenendyk, J., and M. Michalak.** 2005. Endoplasmic reticulum quality control and apoptosis. Acta Biochim. Pol. **52:**381–395.
10. **Haze, K., H. Yoshida, H. Yanagi, T. Yura, and K. Mori.** 1999. Mammalian transcription factor ATF6 is synthesized as a transmembrane protein and activated by proteolysis in response to endoplasmic reticulum stress. Mol. Biol. Cell **10:**3787–3799.
11. **Hirose, H., K. Arasaki, N. Dohmae, K. Takio, K. Hatsuzawa, M. Nagahama, K. Tani, A. Yamamoto, M. Tohyama, and M. Tagaya.** 2004. Implication of ZW10 in membrane trafficking between the endoplasmic reticulum and Golgi. EMBO J. **23:**1267–1278.
12. **Kadowaki, H., H. Nishitoh, and H. Ichijo.** 2004. Survival and apoptosis signals in ER stress: the role of protein kinases. J. Chem. Neuroanat. **28:**93–100.
13. **Klopfenstein, D. R., F. Kappeler, and H. P. Hauri.** 1998. A novel direct interaction of endoplasmic reticulum with microtubules. EMBO J. **17:**6168–6177.
14. **Kuge, O., C. Dascher, L. Orchi, T. Rowe, M. Amherdt, H. Plutner, M. Ravazzola, G. Tanigawa, J. E. Rothman, and W. E. Balch.** 1994. Sar1 promotes vesicle budding from the endoplasmic reticulum but not Golgi compartments. J. Cell Biol. **125:**51–65.
15. **LaPointe, P., C. Gurkan, and W. E. Balch.** 2004. Mise en place—this bud's for the Golgi. Mol. Cell **14:**413–414.
16. **Latterich, M., K. U. Fröhlich, and R. Schekman.** 1995. Membrane fusion and the cell cycle: Cdc48p participates in the fusion of ER membranes. Cell **82:**885–893.
17. **Lee, C., and L. B. Chen.** 1988. Dynamic behavior of endoplasmic reticulum in living cells. Cell **54:**37–46.
18. **Lippincott-Schwartz, J., T. H. Roberts, and K. Hirschberg.** 2000. Secretory protein trafficking and organelle dynamics in living cells. Annu. Rev. Cell Dev. Biol. **16:**557–589.
19. **Marciniak, S. J., and D. Ron.** 2006. Endoplasmic reticulum stress signaling in disease. Physiol. Rev. **86:**1133–1149.
20. **Nakajima, K., H. Hirose, M. Taniguchi, H. Kurashina, K. Arasaki, M. Nagahama, K. Tani, A. Yamamoto, and M. Tagaya.** 2004. Involvement of BNIP1 in apoptosis and endoplasmic reticulum membrane fusion. EMBO J. **23:**3216–3226.
21. **Okada, T., H. Yoshida, R. Akazawa, M. Negishi, and K. Mori.** 2002. Distinct roles of activating transcription factor 6 (ATF6) and double-stranded RNA-activated protein kinase-like endoplasmic reticulum kinase (PERK) in transcription during the mammalian unfolded protein response. Biochem. J. **366:**585–594.
22. **Oyadomari, S., and M. Mori.** 2004. Roles of CHOP/GADD153 in endoplasmic reticulum stress. Cell Death Differ. **11:**381–389.
23. **Patel, S. K., F. E. Indig, N. Olivieri, N. D. Levine, and M. Latterich.** 1998. Organelle membrane fusion: a novel function for the syntaxin homolog Ufe1p in ER membrane fusion. Cell **92:**611–620.
24. **Sato, T., S. Mushiake, Y. Kato, K. Sato, M. Sato, N. Takeda, K. Ozono, K. Miki, Y. Kubo, A. Tsuji, R. Harada, and A. Harada.** 2007. The Rab8 GTPase regulates apical protein localization in intestinal cells. Nature **448:**366–369.
25. **Sok, J., X. Z. Wang, N. Batchvarova, M. Kuroda, H. Harding, and D. Ron.** 1999. CHOP-dependent stress-inducible expression of a novel form of carbonic anhydrase VI. Mol. Cell. Biol. **19:**495–504.
26. **Tajiri, S., S. Yano, M. Morioka, J. Kuratsu, M. Mori, and T. Gotoh.** 2006. CHOP is involved in neuronal apoptosis induced by neurotrophic factor deprivation. FEBS Lett. **580:**3462–3468.
27. **Tang, B. L., F. Peter, J. Krijnse-Locker, S. H. Low, G. Griffiths, and W. Hong.** 1997. The mammalian homolog of yeast Sec13p is enriched in the intermediate compartment and is essential for protein transport from the endoplasmic reticulum to the Golgi apparatus. Mol. Cell. Biol. **17:**256–266.
28. **Uchiyama, K., G. Totsukawa, M. Puhka, Y. Kaneko, E. Jokitalo, I. Dreveny, F. Beuron, X. Zhang, P. Freemont, and H. Kondo.** 2006. p37 is a p97 adaptor required for Golgi and ER biogenesis in interphase and at the end of mitosis. Dev. Cell **11:**803–816.
29. **Uchiyama, K., and H. Kondo.** 2005. p97/p47-mediated biogenesis of Golgi and ER. J. Biochem. **137:**115–119.
30. **Vedrenne, C., D. R. Klopfenstein, and H. P. Hauri.** 2005. Phosphorylation controls CLIMP-63-mediated anchoring of the endoplasmic reticulum to microtubules. Mol. Biol. Cell **16:**1928–1937.
31. **Vedrenne, C., and H. P. Hauri.** 2006. Morphogenesis of the endoplasmic reticulum: beyond active membrane expansion. Traffic **7:**639–646.
32. **Wakana, Y., S. Takai, K. Nakajima, K. Tani, A. Yamamoto, P. Watson, D. J. Stephens, H. P. Hauri, and M. Tagaya.** 2008. Bap31 is an itinerant protein that moves between the peripheral endoplasmic reticulum (ER) and a juxtanuclear compartment related to ER-associated degradation. Mol. Biol. Cell **19:**1825–1836.
33. **Wang, X. Z., and D. Ron.** 1996. Stress-induced phosphorylation and activation of the transcriptional factor CHOP (GADD153) by p38 MAP kinase. Science **272:**1347–1349.
34. **Waterman-Storer, C. M., and E. D. Salmon.** 1998. How microtubules get fluorescent speckles. Biophys. J. **75:**2059–2069.
35. **Yamaguchi, T., A. Yamamoto, A. Furuno, K. Hatsuzawa, K. Tani, M. Himeno, and M. Tagaya.** 1997. Possible involvement of heterotrimeric G proteins in the organization of the Golgi apparatus. J. Biol. Chem. **272:**25260–25266.
36. **Yoshida, H.** 2007. ER stress and diseases. FEBS J. **274:**630–658.